Kinetic Plots for programmed temperature gas chromatography

Sander Jespers[1], Kevin Roeleveld[2], Frederic Lynen[2], Ken Broeckhoven[1], Gert Desmet[1]

[1]*Vrije Universiteit Brussel, Department of Chemical Engineering, Pleinlaan 2, 1050 Brussels, Belgium*

[2] *Universiteit Gent, Separation Science Group, Krijgslaan 281, B-9000 Gent, Belgium*

Corresponding author E-mail: gedesmet@vub.ac.be

Abstract

The applicability of the kinetic plot theory to temperature-programmed gas chromatography (GC) has been confirmed experimentally by measuring the efficiency of a temperature gradient separation of a simple test mixture on 15, 30, 60 and 120 m long (coupled) columns. It has been shown that the temperature-dependent data needed for the kinetic plot calculation can be obtained from isothermal experiments at the significant temperature, a temperature that characterizes the entire gradient run. Furthermore, optimal flow rates have been calculated for various combinations of column length, diameter, and operating temperature (or significant temperature). The tabulated outcome of these calculations provide good starting points for the optimization of any GC separation.

Keywords

1. Introduction

The kinetic plot theory, first developed for LC and recently extended to GC, provides a general framework to compare the quality of different chromatographic systems in a geometry-independent way, as well as to guide system design and determine optimal working conditions [1-4]. In a kinetic plot, a measure for the analysis time (typically the t_0 time, or the time of the last eluting compound) is plotted versus a measure for column efficiency (typically the plate number N or the peak capacity n_p). Whereas in a Van Deemter-plot the length of the column is the same for each data point while the pressure varies, the data points in a kinetic plot all relate to the same maximal, or more generally, optimal pressure drop but to a different column length. Being plotted at the optimal pressure drop, kinetic plots describe, in one single curve, the best performance one can expect from a given chromatographic support (LC) or column diameter (GC) for any possible value of the required efficiency or the allowable analysis time.

Following upon earlier work on the kinetic optimization of GC separations by Giddings [5,6], Cramers [7-9], Blumberg [10,11] and Kurganov et al. [12] , we recently extended the kinetic plot theory from the case of LC (incompressible fluid) to isothermal GC (compressible fluid obeying the ideal gas law). In addition, we also derived the exact equations determining the

59 optimal pressure [4]. Contrary to LC, where the optimal pressure is always the maximum

60 pressure, this optimal pressure is in GC a function of the compound of interest, as well as of

61 the required analysis time. However, the error made by using the maximum pressure drop

62 as the optimal pressure in GC for every compound and column length is rather small. A

63 recent interesting review on the use of kinetic plots for the optimization of separations in LC

64 and GC was published by A.A. Kurganov *et al.* [13].

65 Whereas our previous work related to isothermal GC, many GC measurements are

66 performed under temperature gradient conditions, the focus of this study was to validate

67 the kinetic plot theory for temperature-programmed GC [14-20].

68

2. Experimental

70 All chemicals were HPLC grade from Sigma Aldrich (St. Louis, MO, United States). 4 HP-5MS

71 columns (30 m x 250 μm x 0.25 μm) were obtained from Agilent (Santa Clara, CA, United

72 States). An Agilent 6890 gas chromatograph with FID detector and split/split less injection

73 was used. The H_2 carrier gas was supplied by a Parker Balston Hydrogen Generator H2PD-

74 300-220 (Haverhill, MA, United States). Polyimide sealing resin from Grace Davison

75 Discovery Sciences (Columbia, MD, United States) and universal 2-way fused silica unions

76 from Agilent were used to couple the columns according to the included instructions.

77 The test mixture consisted of ethyl-caprate, tridecane and pentadecane dissolved in 2,2,4-

78 trimethylpentane at a concentration of 50 ppm for each component. A headspace sample

79 was made to determine the elution time of 2,2,4-trimethylpentane (t_M-compound), while a

80 separate sample of 50 ppm was made for each of the three components to determine their

81 elution order.

82 Injection of 1 μL sample was done at 250 °C and a 20:1 split ratio. Separations were

83 performed under gradient conditions with the flow varying between 0.2 – 5.2 mL/min and

84 the oven temperature running form 80 – 200 °C at 10 °C/min for the run at 2.4 mL/min. For

85 the runs at other flow rates, the gradient time was scaled proportionally to the void time.

86 The detector temperature was set at 300 °C, H_2 flow at 40 mL/min, air flow at 300 mL/min

87 and makeup flow at 20 mL/min. Data was analyzed with HPCore ChemStation.

88   Measurements on the 120 m column were performed using a mixture containing 100 ppm of

89   each component and a split ratio of 10:1 to increase the signal intensity.

3. Theory

90

91   A kinetic plot extrapolates the observed efficiency of a given column (with a certain length

92   and stationary phase), measured in the form of a Van Deemter curve, to the expected

93   efficiencies of the same column but at different lengths and all operated at the optimal

94   pressure. A necessary condition for this theory to be valid is that the peak elution pattern is

95   preserved when the column length is changed (i.e., that all peaks retain their relative elution

96   time). In gas chromatography with H_2 as carrier gas the logarithm of the retention factor k is

97   inversely proportional to the carrier gas inlet pressure, however in the range of inlet

98   pressures used in this work (and most GC experiments) this dependency is negligible [21].

99   For isothermal GC the necessary condition is thus met simply by running all measurements

100   at the same temperature. For temperature gradient GC, it is shown in [22] that scaling the

101   gradient time proportionally to the void time leads to a constant peak elution pattern.

102

3.1 Kinetic plot expressions

103

104   The general theory for kinetic plots in GC was introduced, and checked for the isothermal

105   case, in a previous paper [4]. It was shown that the kinetic performance limit (KPL) of a given

106   chromatographic system can be calculated by scaling each of the different performance

107   characteristics: length (L), column void time (t_M), and peak capacity (n_p) with a specific

108   elongation factor.

109    $$L_{KPL} = \lambda_1 L_{exp} \tag{1}$$

110    $$t_{M,KPL} = \lambda_2 t_{M,exp} \tag{2}$$

111    $$n_{p,KPL} = 1 + \sqrt{\lambda_3}\left(n_{p,exp} - 1\right) \tag{3}$$

112   This column elongation-based approach is based on the direct physical interpretation of the

113   column length extrapolation process needed to arrive at the kinetic performance limit of a

114   given chromatographic system, transforming a given peak capacity ($n_{p,exp}$) obtained in a

115   given time $t_{M,exp}$ on a column with length L_{exp} and producing a given pressure drop Δp_{exp} into

116   the peak capacity one can expect in a column producing the optimal pressure drop Δp_{opt}

117   while keeping the same mobile phase outlet velocity (and hence having an adapted length

118   L_{KPL}).

119   Whereas in LC the expressions for λ are very simple [3], the expressions for the pressure

120   dependency of the λ–elongation factors for thin-film GC are more complex, and have in [4]

121   been shown to be given by:

122
$$\lambda_1 = \frac{\Delta p_{opt} \dfrac{(P_{opt}^2-1)}{(P_{opt}-1)}}{\Delta p_{exp} \dfrac{(P_{exp}^2-1)}{(P_{exp}-1)}} = \left[\frac{\Delta p_{opt}}{\Delta p_{exp}}\right] \frac{f_{0,exp}}{f_{0,opt}} \tag{4}$$

123
$$\lambda_2 = \frac{\Delta p_{opt} \dfrac{(P_{opt}^3-1)}{(P_{opt}-1)}}{\Delta p_{exp} \dfrac{(P_{exp}^3-1)}{(P_{exp}-1)}} = \left[\frac{\Delta p_{opt}}{\Delta p_{exp}}\right] \frac{f_{4,opt}}{f_{4,exp}} \tag{5}$$

124
$$\lambda_3 = \frac{\Delta p_{opt} \dfrac{(P_{opt}^3-1)^2}{(P_{opt}^4-1)(P_{opt}-1)}}{\Delta p_{exp} \dfrac{(P_{exp}^3-1)^2}{(P_{exp}^4-1)(P_{exp}-1)}} = \left[\frac{\Delta p_{opt}}{\Delta p_{exp}}\right] \frac{f_{3,opt}}{f_{3,exp}} \tag{6}$$

125   Where Δp is the pressure drop over the column, P is the ratio of inlet pressure to outlet

126   pressure, and the subscripts "opt" and "exp" refer to the optimal and experimental values

127   respectively.

128   ### 3.2 Determining the optimal pressure

129   Whereas in LC the pressure leading to the kinetic performance limit is always equal to the

130   maximal available pressure, it was previously shown [4] that the optimal pressure drop for

131   any given thin-film GC column is determined by the following cubic equation:

132
$$\Delta p_{exp}^3 + \alpha \Delta p_{exp}^2 - \beta = 0 \tag{7}$$

133   With $\alpha = 3p_{o,exp}$, $\beta = \dfrac{6B'p_{o,exp}^2}{C_m'}$, $B' = \dfrac{B}{p_{o,exp}}\sqrt{\dfrac{\eta t_M}{K_v}}$ and $C_m' = C_m p_{o,exp}\sqrt{\dfrac{K_v}{\eta t_M}}$,

134   With η the viscosity of the mobile phase, K_v the column permeability, p_o the outlet pressure,

135   and B and C_m the constants in the equation giving the observed plate height in thin film GC

136   as a function of outlet velocity u_o:

137    $$H_{obs} = \left(\frac{B}{u_o p_o} + C_m u_o p_o \right) \cdot \frac{9(P_{exp}^4 - 1)(P_{exp}^2 - 1)}{8(P_{exp}^3 - 1)^2} \tag{8}$$

138   Calculating the roots of this cubic equation, as previously described in [4], we obtain one real

139   and two complex roots:

140    $$\Delta p_{opt,1} = \frac{1}{3} \left[\frac{\sqrt[3]{3\sqrt{3}\sqrt{27\beta^2 - 4\beta\alpha^3} + 27\beta - 2\alpha^3}}{\sqrt[3]{2}} + \frac{\sqrt[3]{2}\alpha^2}{\sqrt[3]{3\sqrt{3}\sqrt{27\beta^2 - 4\beta\alpha^3} + 27\beta - 2\alpha^3}} - \alpha \right]$$

141   (9)

142    $$\Delta p_{opt,2} = -\frac{(1 - i\sqrt{3})\sqrt[3]{3\sqrt{3}\sqrt{27\beta^2 - 4\beta\alpha^3} + 27\beta - 2\alpha^3}}{6\sqrt[3]{2}}$$
$$-\frac{(1 + i\sqrt{3})\alpha^2}{3\sqrt[3]{4}\sqrt[3]{3\sqrt{3}\sqrt{27\beta^2 - 4\beta\alpha^3} + 27\beta - 2\alpha^3}} - \frac{\alpha}{3} \tag{10}$$

143    $$\Delta p_{opt,3} = -\frac{(1 + i\sqrt{3})\sqrt[3]{3\sqrt{3}\sqrt{27\beta^2 - 4\beta\alpha^3} + 27\beta - 2\alpha^3}}{6\sqrt[3]{2}}$$
$$-\frac{(1 - i\sqrt{3})\alpha^2}{3\sqrt[3]{4}\sqrt[3]{3\sqrt{3}\sqrt{27\beta^2 - 4\beta\alpha^3} + 27\beta - 2\alpha^3}} - \frac{\alpha}{3} \tag{11}$$

144   As stated in [4] Δp_{opt} is a function of the mobile phase residence time t_M via the factor β. For

145   low t_M-values (up to the inflection point), only the $\Delta p_{opt,1}$-root is a real number and is the one

146   to be used. For larger t_M-values (after the inflection point), the $\Delta p_{opt,2}$-root becomes the

147   single real root. Note that the inflection point (i.e. the t_M-value at which the $\Delta p_{opt,1}$-root

148   becomes an imaginary number, and the $\Delta p_{opt,2}$-root becomes a real number) is also a

149   function of α and β, and thus changes when the considered column or compound is changed

150   [4]. The root $\Delta p_{opt,3}$ relates to a physically impossible solution involving a decreasing optimal

151   pressure drop for an increasing t_M. When the calculated optimal pressure drop exceeds the

152   maximum pressure drop of the system, Δp_{opt} needs to be taken equal to Δp_{max}.

153   ## 3.3 Determining Van Deemter constants for gradient runs

154   The values for B, C_m, and η needed in Eqs. (7-10) cannot be determined via gradient

155   measurements as they are functions of temperature. However, representative values for B

156 and C_m of a given compound and η for a given mobile phase can be obtained from

157 isothermal Van Deemter data at the so-called significant temperature T' of that compound

158 using that mobile phase [24]. This significant temperature, as defined by Giddings, is the

159 temperature of the isothermal run that characterizes the entire gradient range (i.e., the

160 temperature that would lead to the same amount of peak spreading and the same degree of

161 separability in an isothermal run as is obtained with the gradient run). Assuming that the

162 influence of a given temperature range is proportional to the distance migrated by the peak

163 in this range, Giddings determined that T' can be approached as a weighted average

164 temperature and would be much closer to the elution temperature than to the starting

165 temperature. As shown by Giddings [24], this significant temperature T' can be found from:

166
$$T^{'} = T_r - \frac{3\,\Delta T}{2} \qquad (12)$$

167 With T_r the elution temperature (the actual temperature at which elution occurs), ΔT the

168 increase in temperature needed to double the fraction of total solute found in the vapor

169 phase and given by:

170
$$\Delta T = 0.693 \frac{RT_{av}^2}{\Delta H_v} \qquad (13)$$

171 Where $\Delta H_v/T_{av}$ can be approximated by 86 Joule mol^{-1} K^{-1}, R = 8.314 Joule K^{-1} mol^{-1} and T_{av} is

172 the geometric mean of the operating temperatures.

173

3.4 Optimal flow rates

175 Knowledge of the optimal pressure allows for the theoretical prediction of the optimal time-

176 efficiency combinations constituting the kinetic performance limit curve. In order to be

177 useful in practice, these optimal pressures have to be transformed to optimal flows, because

178 temperature gradient experiments are generally performed under constant flow conditions.

179 This transformation can be made starting from a chosen series of t_M and calculating for each

180 t_M the corresponding Δp_{opt} using Eqs. (7-10). From this data, the optimal column length

181 corresponding to each t_M can be found from [4, supplementary material]:

182 $$L_{opt} = \sqrt{\Delta p_{opt} K_v t_M \frac{3(P_{opt}^2 - 1)(P_{opt} + 1)}{4\eta(P_{opt}^3 - 1)}}$$ (14)

183 From the (t_M, L_{opt})-data sets, the optimal outlet velocity $(u_{o,opt})$ and flow rate (F) can be

184 calculated via [8]:

185 $$u_{o,opt} = \frac{L_{opt}}{t_M} \cdot \frac{2(P_{opt}^3 - 1)}{3(P_{opt}^2 - 1)}$$ (15)

186 And using the column inner diameter (d_c)

187 $$F_{opt} = \frac{\pi d_c^2}{4} \cdot u_{o,opt}$$ (16)

188

4. Results and discussion

4.1 Efficiency measurements

191 Fig. 1 shows an example of the gradient separation on the 15m long column at the optimal

192 flow for pentadecane (2.3 mL/min). The peak capacity, calculated on the basis of the peak

193 width and retention time of the last eluting compound, was used as a measure for the

194 gradient efficiency and corresponded to 288.7. Similar separations were obtained on the 30,

195 60, and 120m long columns at 2, 1.8, and 1.3 mL/min resulting in peak capacities of 363.3,

196 512.1, and 696.5, respectively.

4.2 Validation of the kinetic plot extrapolation

198 Fig. 2a shows the experimental data points (black dots) for pentadecane obtained on the 30

199 m long column, the corresponding fit (full line), and the extrapolation to the kinetic

200 performance limit using Eqs.(2,3) for the experimental data points (black triangles) and the

201 fit (dashed line). The fits are made using Eq. (20), see further. The square data points

202 represent the experimental verification measurements at the optimal flow carried out on

203 the 15, 30, 60 and 120 m long columns to verify the proposed gradient GC-kinetic plot theory

204 (each data point is average of 3 measurements). As can be noted, the experimental data

205 points coincide well with the kinetic performance limit predictions for the 15, 30 and 60 m

206 long columns. There is a significant deviation for the 120 m long column (9% difference

207 between the predicted n_p and the measured n_p), but this is essentially due to a change in the

208 retention factor of pentadecane at these measurements caused by the fact that the flow
209 rate on the instrument can only be set with an increment of 0.1 mL/min. The associated
210 rounding errors cause corresponding differences in the gradient steepness. These have a
211 higher impact on the measurements on long columns since these are performed at lower
212 flow rates.

213 The fitted curve running through the data points on the 30 m long column is obtained by
214 transforming the peak capacities into the quantity $(n_p-1)^{-2}$. This quantity exhibits the same
215 velocity-dependency as that governing the plate-height equation. This can be shown starting
216 from the well-established relation between the peak capacity and the plate number [23]

217 $$n_p = 1 + \sqrt{N} \cdot \psi \tag{17}$$

218 Where ψ is a constant for a given experimental set up and only depends on the
219 dimensionless heating rate, which is furthermore the same for all experiments. This equation
220 can be transformed into a form relating n_p to H as:

221 $$\Rightarrow \sqrt{N} = \frac{(n_p - 1)}{\psi} \tag{18}$$

222 $$\Rightarrow H = \frac{L}{N} = \frac{L \psi^2}{(n_p - 1)^2} \tag{19}$$

223 $$\Rightarrow \frac{1}{(n_p - 1)^2} = \frac{\beta}{p_o u_o} + \gamma p_o u_o \tag{20}$$

224

225 wherein the constants β and γ are equivalent to B and C_m from the plate height equation,
226 but without the same physical meaning (e.g. proportional to L).

227 The difference between working at the optimal pressure drop and working at the maximum
228 pressure drop is shown in Fig 2b. The fact that Δp_{opt} is lower than Δp_{max} for the 15, 30, and
229 60 m long columns implies that it should always be possible to realize a gain in n_p (or a
230 decrease in analysis time) by switching to a shorter column operated at this lower pressure
231 drop Δp_{opt} compared to working with a longer column operated at Δp_{max}. As can be noted,
232 this is indeed the case. For example, a 15m column operated at Δp_{opt} has a more than 25%
233 higher peak capacity than a 30m column at Δp_{max} in roughly the same analysis time and a

234 30m column at Δp_{opt} has the same peak capacity as a 60m column at Δp_{max} but in a 35%

235 shorter analysis time. For the measurements on the 120 m long column, the calculated Δp_{opt}

236 (according to Eqs. (9,10)) exceeded the maximum pressure drop, hence $\Delta p_{opt} = \Delta p_{max}$. As a

237 consequence, only one data point is considered here (*vide supra* for the deviation of this

238 point from the dashed curve).

239 In Fig. 3a, the kinetic plot for the entire sample was constructed, calculating the peak

240 capacity on the basis of the widths of all the peaks, according to [23]:

241 $$n_p = 1 + \sum_{i=1}^{n} \frac{t_{R,i} - t_{R,i-1}}{4\sigma_{t,i}} \qquad (21)$$

242 The optimal pressure for the entire sample, which differs from that for an individual

243 component (case considered in Fig. 2), was determined starting from isothermal Van

244 Deemter data obtained on a 30 m long column at the average of the elution temperatures T_r

245 of the components in the gradient experiments (in this case 100 °C) . The values for B and C_m

246 in Eqs.(9,10) for the optimal pressure were found by fitting the average of this Van Deemter

247 data set. This average Van Deemter data was calculated by taking, for each velocity, the

248 square of the plate number (since the actual resolution of a separation is determined by N²).

249 This was first done for each component separately. Subsequently the mean of these values

250 was taken (per velocity data point), and then the column length was divided by the square

251 root of this mean. The viscosity needed for these equations was also determined at this

252 mean elution temperature.

253 Finally, calculating λ_2 and λ_3 by using the optimal pressure drop values (which are, due to the

254 dependency on the B and C_m term, specific for the considered component/mixture) in Eqs.

255 (5-6), and subsequently applying Eqs. (2-3) to the experimental (t_M, n_p)-data set, the kinetic

256 plot for the entire sample can be calculated.

257 Fig. 3b shows the kinetic plot for the sample (dashed line), constructed as described above,

258 and experimental measurements on a 15 m (blue markers), 30 m (green markers), 60 m

259 (black markers), and 120 m (red markers) long column. These experimental data points

260 represent the peak capacity for the entire sample (calculated using Eq. 21), obtained by

261 applying the optimal pressure corresponding to a specific component (tridecane: diamonds,

262 ethyl caprate: circles, pentadecane: triangles). On the 60 m column the measurements for

263   ethyl caprate and pentadecane are almost identical, hence it appears only 2 data points are

264   shown. As expected, when the peak capacity for the entire sample is concerned, optimizing

265   the pressure for the sample yields a curve that is the best compromise between optimizing

266   the pressure for tridecane, ethyl caprate, or pentadecane.

267   Although a sample with only limited complexity is considered, the chosen compounds cover

268   a big range in variation of B and C_m values. B is compound specific through D_{mol}, which only

269   varies a factor of 3 over the range C_5-C_{40}, and only a factor of 1.5 over the range C_{20}-C_{40} for

270   the n-alkanes [25]. C_m is compound specific through D_{mol} and the term $\vartheta_{G1}^2=$

271   $(1+6k+11k^2)/(1+k)^2$, where k is the retention factor of the compound. As k changes from 0 to

272   infinity ϑ_{G1}^2 rises asymptotically from 1 to approximately 10.89, reaching a value of 9 at k =7.

273   Between the chosen compounds D_{mol} varies up to approximately a factor of 1.5 and ϑ_{G1}^2

274   changes from 1 to approximately 9. Furthermore, since it has been shown [25] that the

275   diffusivity of a member of the n-alkanes represents the diffusivity of all possible solutes

276   eluting closely with it, the range of variation in D_{mol} (and thus B and C_m) is thus not limited to

277   n-alkanes alone but representative for all solute classes.

4.3 Optimized flow for different experimental conditions

279   Since the optimal pressure depends on the specific B- and C_m-values for each component,

280   different kinetic plots are obtained for each component. However, as shown in Fig. 4, all

281   these kinetic plots coincide over a large range of peak capacities. The difference is only

282   notable at very high peak capacities (and thus very long columns/slow experiments). Thus,

283   for practical applications, which are typically not performed in this high peak capacity region,

284   there is no difference between the optimization using different compounds.

285   Based on the B- and C_m-values of a given compound, and since it is known how the B- and

286   C_m-values depend on temperature and column diameter, the optimal flow can be

287   determined for any possible column length and any possible isothermal oven temperature

288   (or compound significant temperature [24]) using Eqs. (9,10) and (14-16) and this for

289   different column diameters. This approach leads in many cases to values that are equivalent

290   to the findings of L.M. Blumberg, who suggested that, independent of column length or

291   temperature, the optimal ratio of flow rate over column diameter equals 8-10 mL min^{-1}

292   mm$_{diameter}^{-1}$ [25].

293 The data presented in Table 1 provides a more detailed view of the dependency of the

294 optimal flowrate (F_{opt}) based on the B- and C_m-values of the entire sample on column

295 diameter, length, and operating temperature (or compound significant temperature). It is

296 shown that, in most common cases, indeed the optimal flowrate is approximately equal to 8-

297 10 mL min^{-1} mm$_{diameter}$$^{-1}$ (cf. the red box delimiting the "Blumberg"-solutions), while for the

298 more extreme cases of column length and operating temperature the optimal flow rate

299 tends to deviate from this guideline. As discussed in previous work [4], this difference results

300 from the pressure drop information which is included in the kinetic plot theory, whereas

301 L.M. Blumberg assumes no pressure drop limitations [22]. Hence, optimal flow rate is a

302 function of column length in the kinetic plot theory, while it is independent of column length

303 in L.M. Blumberg's work. This observation is important for both the µGC field as well as the

304 GC x GC field. µGC columns are typically narrow and short (max 5 m) and are, due to the

305 glues used to fix the capillaries, operated at lower temperatures. In GC x GC, the second

306 dimension columns are typically narrow and short (1-2 m) in order to maintain the

307 separation by the primary column.

308 The experimental verification of the flow rates in Table 1 is presented in Fig. 3 and Fig. 4. In

309 Fig. 4 it is shown that using the parameters of a specific compound or the entire sample

310 leads to almost identical kinetic plots (and thus optimal flows), in Fig 3 it is shown that

311 experimental measurements on the 15, 30, 60, and 120m long columns at the optimal flow

312 rates for the specific compounds coincide well with the predicted curve. In other words, the

313 values in Table 1-b at 100 °C and L = 15, 30, 60, and 120m were experimentally verified.

314 It is also shown (Table 2) that using the t_M-compound in the calculations leads to optimal

315 flows which are roughly two times higher than those obtained when using the other

316 compounds (or the sample as a whole). This can be explained by the extreme values of D_{mol}

317 and ϑ_{G1}^2 found for the t_M-compound as compared to the values of the solutes. As previously

318 described, D_{mol} for the t_M-compound is up to a factor of 1.5 higher than the D_{mol} of the

319 solutes, while the ϑ_{G1}^2 term of the t_M-compound is up to a factor of 9 lower.

5. Conclusions

321 It is shown experimentally that the kinetic plot theory for GC, previously developed for

322 isocratic conditions [4], is also applicable to temperature-programmed GC, provided that the

323 peak capacity is used as a measure for efficiency, and that the gradient time is scaled

324 proportionally to the void time to preserve the peak elution pattern. We only observed a

325 discrepancy between theoretical prediction and experimental verification at very long

326 column lengths (120m), but these can be attributed to the rounding errors on the imposed

327 flow rate of the instrument.

328 It is furthermore shown that the Van Deemter data needed to calculate the optimal pressure

329 for temperature-programmed GC separations can be found from isothermal Van Deemter

330 measurements at the significant temperature (as defined in [24]).

331 Optimal pressures were calculated for a range of column lengths, diameters, and operating

332 temperature (or compound significant temperature) and, for practical use, translated into

333 optimal flow rates. These optimal flow rates, although specific for the sample used in this

334 work, can be used as starting points in the optimization of other separations. For the most

335 common combinations of length, diameter, and temperature the proposed optimal flow

336 rates are equal to the guideline proposed by L.M. Blumberg, who stated that, independent

337 of column length or temperature, the optimal ratio of flow rate over column diameter

338 equals 8-10 mL min^{-1} $mm_{diameter}^{-1}$. For the more divergent cases the proposed optimal flow

339 rates deviate from this guideline.

340

6. Acknowledgement

References

345 [1] G. Desmet, D. Clicq, P. Gzil, Geometry-independent plate height representation methods

346 for the direct comparison of the kinetic performance of LC supports with different size or

347 morphology, Anal. Chem. 77 (2005) 4058-4070.

348 [2] G. Desmet, P. Gzil, D. Clicq, Kinetic plots to directly compare the performance of LC

349 supports, LC GC Eur. 7 (2005) 403-409.

[3] K. Broeckhoven, D. Cabooter, F. Lynen, P. Sandra, G. Desmet, The kinetic plot method applied to gradient chromatography: theoretical framework and experimental validation, J. Chromatogr. A 1217 (2010) 2787-2795.

[4] S. Jespers, K. Roeleveld, F. Lynen, K. Broeckhoven, G. Desmet, Kinetic plots for gas chromatography: theory and experimental verification, J. Chromatogr. A 1386 (2015) 81-88.

[5] J.C. Giddings, Comparison of theoretical limit of separating speed in gas and liquid chromatography, Anal. Chem. 37 (1965) 60-63.

[6] J.C. Giddings, Theory of minimum time operation in gas chromatography, Anal. Chem. 34 (1962) 314-319.

[7] C.P.M. Schutjes, P.A. Leclercq, J.A. Rijks, C.A. Cramers, Model describing the role of the pressure gradient on efficiency and speed of analysis in capillary gas chromatography, J. Chromatogr. 289 (1984) 163-170.

[8] C.A. Cramers, H.G. Janssen, M.M van Deursen, P.A. Leclercq, High-speed gas chromatography: an overview of various concepts, J. Chromatogr. A 856 (1999) 315-329.

[9] C.A. Cramers, P.A. Leclercq, Statregies for speed optimisation in gas chromatography : an overview, J. Chromatogr. A 842 (1999) 3-13.

[10] L.M. Blumberg, Theory of fast capillary gas chromatography part 1: column effiency, J. High Resol. Chromatogr. 20 (1997) 597-604.

[11] L.M. Blumberg, Theory of fast capillary gas chromatography part 2: speed of analysis, J. High Resolut. Chromatogr. 20 (1997) 679-687.

[12] A.A. Kurganov, A.A. Korolev, V.E. Shiryaeva, T.P. Popova, A.Yu. Kanateva, Kinetic effiency of polar monolithic capillary columns in high-pressure gas chromatography, J. Chromatogr. A 1315 (2013) 162-166.

[13] A.A. Kurganov, A. Kanateva, E. Yakubenko, Application of kinetic plots in gas and liquid chromatography for the optimization of separation conditions, J. Sep. Sci. 39 (2016) 162-176.

[14] B. Savareear, M.R. Jacobs, R.A. Shellie, Multiplexed dual first-dimension comprehensive two-dimensional gas chromatography- mass spectrometry with contra directional thermal modulation, J. Chromatogr. A 1365 (2014) 183-190.

378 [15] M. Pursch, P. Eckerle, J. Biel, R. Streck, H. Cortes, K. Sun, Comprehensive two-
379 dimensional gas chromatography using liquid nitrogen modulation: set-up and applications,
380 J. Chromatogr. A 1019 (2003) 43-51.

381 [16] V. Jain & J. B. Phillips, High-speed gas chromatography using simultaneous temperature
382 gradients in both time and distance along narrow-bore capillary columns, J. Chromatogr. Sci
383 33 (1995) 601-605.

384 [17] J.B. Phillips & V. Jain, On-column temperature programming in gas chromatography
385 using temperature gradients along the capillary column, J. Chromatogr. Sci 33 (1995) 541-
386 550.

387 [18] S.A. Mjøs, Identification of fatty acids in gas chromatography by application of different
388 temperature and pressure programs on a single capillary column, J. Chromatogr. A 1015
389 (2003) 151-161.

390 [19] R.L. Grob & E.F. Barry, Modern practice of gas chromatography, Wiley, Weinheim,
391 2004.

392 [20] C. Cheng, S. Liu, B.J. Mueller, Z. Yan, A generic static headspace gas chromatography
393 method for determination of residual solvents in drug substance, J. Chromatogr. A 1217
394 (2010) 6413-6421.

395 [21] A.V. Kozin, A.A. Korolev, V.E. Shiryaeva, T.P. Popova, A.A. Kurganov, The influence of the
396 natures of the carrier gas and the stationay phase on the separating properties of monolithic
397 capillary columns in gas adsorption chromatography, Russ. J. Phys. Chem. A 82 (2008) 276-
398 281.

399 [22] L.M. Blumberg, M.S.Klee, Method translation and retention time locking in partition GC,
400 Anal. Chem. 70 (1998) 3828-3839.

401 [23] E. Grushka, Chromatographic peak capacity and the factors influencing it, Anal. Chem.
402 42 (1970) 1142-1147.

403 [24] J.C. Giddings, Elementary theory of programed temperature gas chromatography, J.
404 Chem. Educ. 39 (1962) 569-573.

405   [25] L.M. Blumberg, Temperature-programmed gas chromatography, Wiley, Weinheim,

406   2010.

407

Figure captions

Figure 1. Chromatogram of the separation of tridecane (k= 4.0), ethyl-caprate (k= 5.1) and pentadecane (k= 6.2) in 2,2,4-trimethylpentane on the 15 m column at the optimal flow rate for pentadecane. T_{oven}: 80 – 200°C, F = 2.3 mL/min, $t_{gradient}$ = 5.3 min.

Figure 2. (a) Experimental measurements of peak capacity at different flow rates on a 30 m column (circles) and corresponding fit (full line), using Eq. (20). The kinetic plot extrapolations of the experimental data points and fit, with Eqs. (2,3), are represented by the triangles and dashed line, respectively. Experimental measurements on columns of different length, at the optimal flow rates for tridecane, are shown as well (red squares). The peak capacities were calculated using the width of the tridecane peak. **(b)** The kinetic plot for tridecane (dashed line) is shown, as well as experimental measurements at the optimal and the maximum flow for tridecane at each column length (squares) are shown. At 120 m the optimal flow and the maximum flow are equal.

Figure 3. (a) Experimental measurements of the peak capacity of the entire sample at different flow rates on a 30 m column (circles) and the corresponding fit (full line), as well as the kinetic plot extrapolation of the experimental fit (dashed line). **(b)** The kinetic plot extrapolation for the entire sample (dashed line) and experimental measurements on each column length are shown (15m: blue, 30m: green, 60m: black, 120m: red). The experimental data points represent the peak capacities of the entire sample (Eq. (21)), obtained at the optimal flow rate for a specific component (tridecane: diamonds, ethyl caprate: circles, pentadecane: triangles). On the 60 m column the data points for ethyl caprate and pentadecane coincide.

Figure 4. Kinetic plot extrapolations for the peak capacity of the entire sample using the optimal pressures for different components are shown. T_M-compound: black, tridecane: yellow, ethyl caprate: green, pentadecane: red, sample: blue.

437   **Figure 1.**
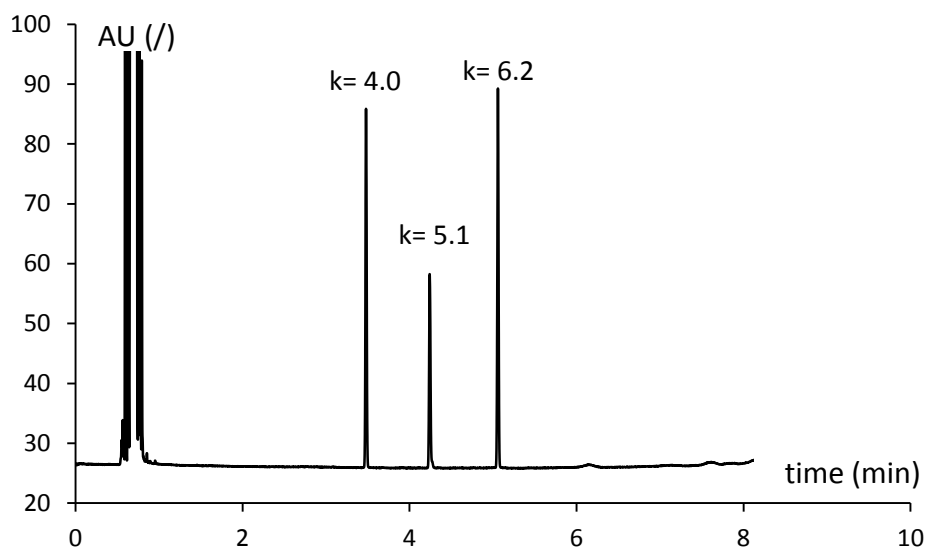
438

439

440

441   **Figure 2a.**
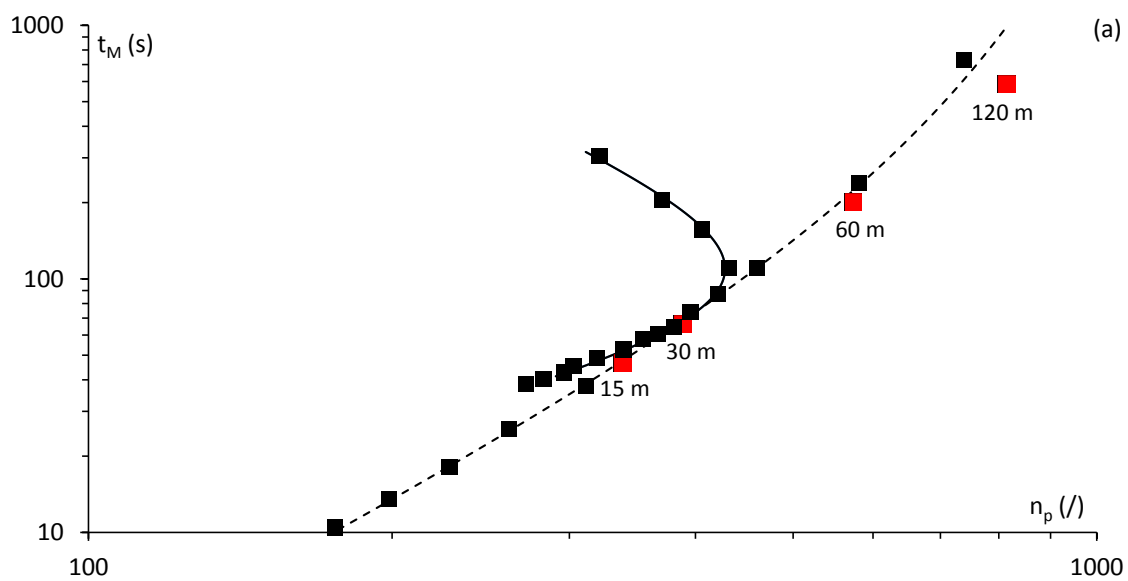
442

443

444

445

446

447   **Figure 2b.**
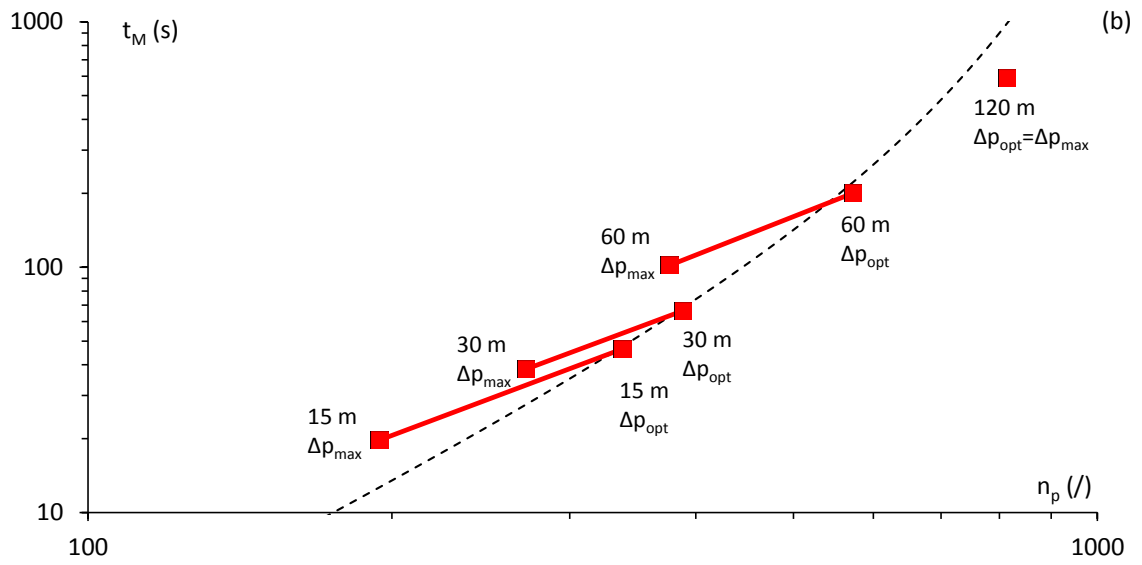
448

449

450

451   **Figure 3a.**
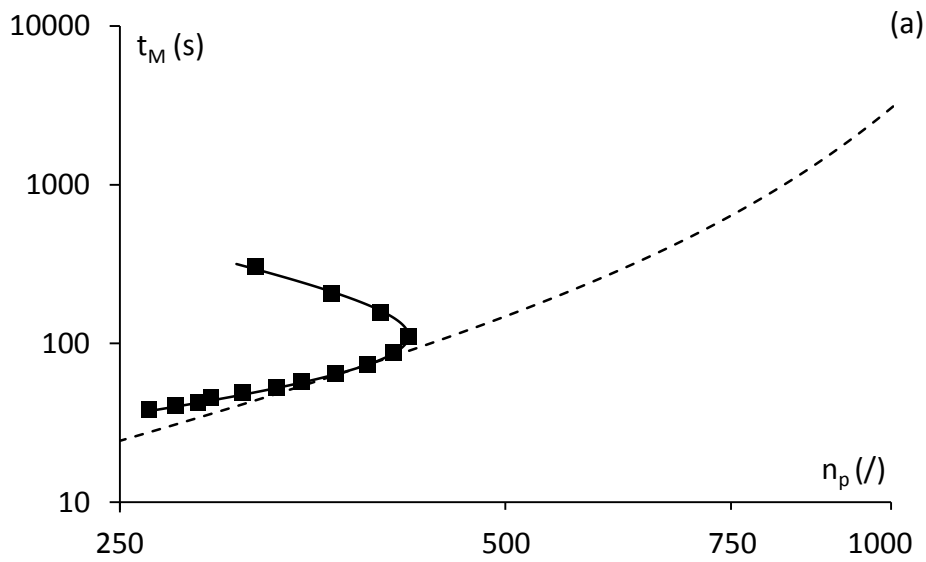
452

453

454

455

456

457 **Figure 3b.**
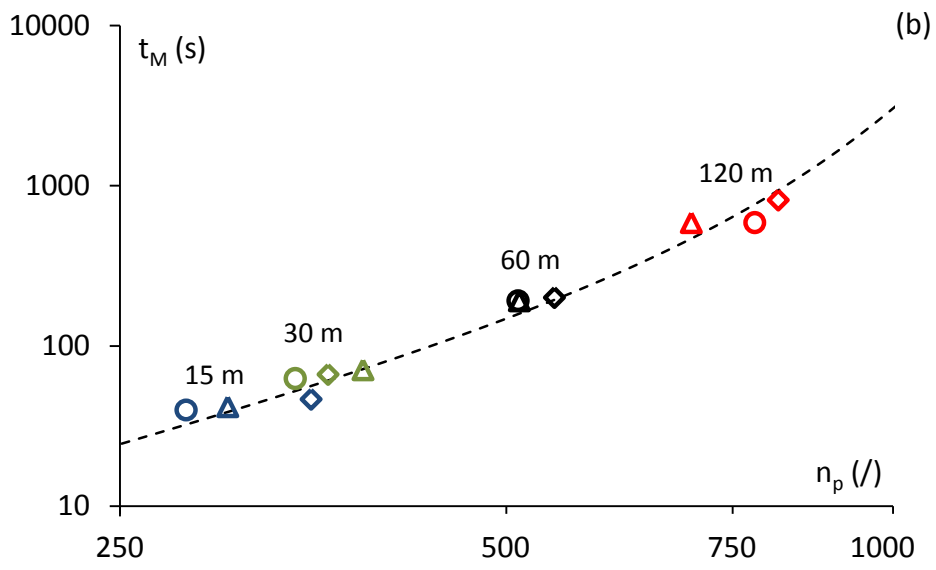
458

459

460

461 **Figure 4.**
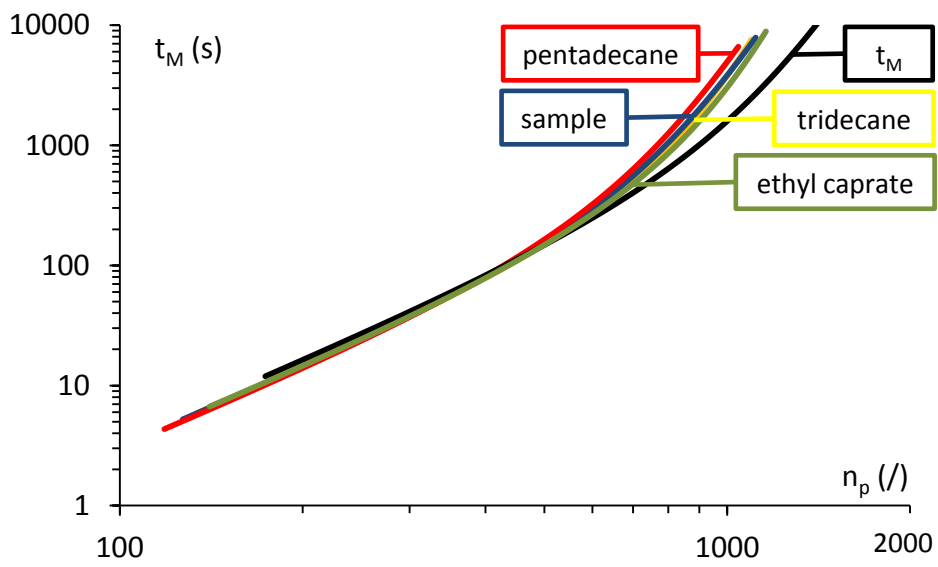
462

463

464

465

466

467

Table 1. Optimal flow rate in mL/min as a function of column length and oven temperature/compound significant temperature for (a) a 100 µm diameter column (b) a 250 µm diameter column (c) a 530 µm diameter column. The calculations were done using Eqs.(9,10) and (14-16) and based on the B- and C_m-values of the entire sample. The red boxes in comprise the cases for which the predictions made by L.M. Blumberg are found.

(a)

L (m)	T (°C)							
	60	80	100	120	150	200	250	300
1	0.9	0.9	1	1.1	1.1	1.3	1.5	1.6
2.5	0.7	0.8	0.8	0.9	0.9	1.1	1.2	1.4
5	0.6	0.7	0.7	0.8	0.9	1	1.1	1.3
10	0.6	0.6	0.7	0.7	0.8	0.9	1.1	1.2
15	0.5	0.6	0.6	0.7	0.8	0.9	1	1.2
30	0.5	0.6	0.6	0.7	0.7	0.9	1	1.2
45	0.5	0.6	0.6	0.7	0.7	0.9	1	1.2
60	0.5	0.6	0.6	0.7	0.7	0.9	1	1.2
90	0.5	0.6	0.6	0.7	0.7	0.9	1	1.1
120	0.5	0.6	0.6	0.7	0.7	0.9	1	1.1

(b)

L (m)	T (°C)							
	60	80	100	120	150	200	250	300
1	4.8	5.1	5.4	5.7	6.1	6.8	7.5	8.1
2.5	3.7	3.9	4	4.2	4.5	4.9	5.4	5.8
5	3	3.2	3.4	²3.6	3.8	4.3	4.7	5.2
10	2.3	2.4	2.6	2.7	2.9	3.3	3.6	4
15	2.1	2.2	2.2	2.4	2.7	3	3.4	3.7
30	1.8	1.9	2	2.1	2.3	2.7	3	3.4
45	1.7	1.8	1.9	2	2.2	2.5	2.9	3.2
60	1.6	1.7	1.8	1.9	2.1	2.5	2.8	3.2
90	1.5	1.6	1.7	1.9	2	2.4	2.7	3.1
120	1.5	1.6	1.7	1.8	2	2.3	2.7	3

(c)

L (m)	T (°C)							
	60	80	100	120	150	200	250	300
1	21.2	22.4	23.7	24.9	26.7	29.6	32.3	35
2.5	15.9	16.7	17.4	18.1	19.1	20.8	22.4	24
5	12.8	13.6	14.3	15	16	17.7	19.4	21
10	9.2	9.7	10.2	10.6	11.3	12.5	13.6	14.7
15	8	8.5	8.9	9.3	10	11	12.2	13.3
30	6.5	6.9	7.2	7.6	8.2	9	9.9	11
45	5.8	6.1	6.5	6.8	7.3	8.1	9	9.9
60	5.4	5.7	6	6.3	6.8	7.6	8.5	9.3
90	4.8	5.1	5.4	5.7	6.2	7	7.8	8.6
120	4.5	4.8	5.1	5.4	5.8	6.6	7.4	8.2

Table 2. Optimal flow rate in mL/min as a function of column length and oven temperature/compound significant temperature for (a) a 100 µm diameter column (b) a 250 µm diameter column (c) a 530 µm diameter column. The calculations were done using Eqs.(9,10) and (14-16) and based on the B-and C_m-values of the t_M marker.

(a)

L (m)	T (°C)							
	60	80	100	120	150	200	250	300
1	1.6	1.7	1.9	2	2.1	2.4	2.7	3.1
2.5	1.3	1.4	1.5	1.7	1.8	2.1	2.4	2.7
5	1.3	1.4	1.5	1.6	1.7	2	2.3	2.6
10	1.2	1.3	1.4	1.5	1.6	1.9	2.2	2.5
15	1.1	1.2	1.3	1.5	1.6	1.9	2.2	2.5
30	1.1	1.2	1.3	1.4	1.6	1.9	2.2	2.5
45	1.1	1.2	1.3	1.4	1.6	1.9	2.2	2.5
60	1.1	1.2	1.3	1.4	1.6	1.9	2.2	2.5
90	1.1	1.2	1.3	1.4	1.6	1.9	2.2	2.5
120	1.1	1.2	1.3	1.4	1.6	1.9	2.2	2.5

490   (b)

L (m)	T (°C)							
	60	80	100	120	150	200	250	300
1	8.5	9	9.4	9.9	10.5	11.6	12.7	13.8
2.5	6	6.3	6.6	6.9	7.4	8.2	9	9.9
5	5.4	5.7	6	6.3	6.8	7.6	8.4	9.2
10	4.1	4.4	4.7	5.1	5.5	6.4	7.2	8.1
15	3.8	4.1	4.3	4.6	5	5.7	6.5	7.3
30	3.4	3.6	3.9	4.2	4.6	5.3	6	6.8
45	3.2	3.5	3.7	4	4.4	5.1	5.8	6.6
60	3.1	3.4	3.6	3.9	4.3	5	5.7	6.5
90	3	3.3	3.5	3.8	4.2	4.9	5.6	6.4
120	3	3.2	3.5	3.7	4.1	4.8	5.6	6.4

491

492   (c)

L (m)	T (°C)							
	60	80	100	120	150	200	250	300
1	37	38.9	40.7	42.5	45.2	49.5	53.7	57.7
2.5	25.1	26.2	27.3	28.3	29.9	32.5	35.1	39.3
5	22	23.1	24.2	25.3	26.9	29.5	32.1	34.7
10	15.9	17	18.1	19.2	20.8	23.5	26.1	28.7
15	13.9	14.7	15.4	16.2	17.4	19.3	21.3	23.2
30	11.3	12	12.5	13.4	14.4	16.2	18	19.8
45	10.2	10.8	11.5	12.1	13.1	14.8	16.5	18.1
60	9.5	10.2	10.7	11.4	12.3	14	15.6	17.4
90	8.7	9.3	9.9	10.5	11.4	13	14.6	16.3
120	8.2	8.8	9.4	9.9	10.9	12.4	14	15.7

493

494

495